Proceedings of the Twelfth International Conference on
Engineering Computational Technology
Edited by: P. Iványi, J. Kruis and B.H.V. Topping
Civil-Comp Conferences, Volume 8, Paper 5.5
Civil-Comp Press, Edinburgh, United Kingdom, 2024
ISSN: 2753-3239, doi: 10.4203/ccc.8.5.5

A semi-explicit dynamic phase field model with domain decomposition based on dual partition super-elements

Y. Chen and B. A. Izzuddin

Department of Civil and Environmental Engineering
Imperial College London
United Kingdom

Abstract

The phase field model has gained popularity in recent years as an elegant way to model fracture but suffers from issues of solvability and high computational cost. In this study, its computational efficiency is improved by extending a domain decomposition method that utilises dual partition super elements. This approach requires no additional parameters and is easily adaptable with minimal modifications. Furthermore, a semi-explicit integration scheme is developed as a robust method for tracing the dynamic equilibrium path. It is demonstrated based on the numerical example of a single notched plate that combining the semi-explicit scheme with the domain decomposition method can achieve significant speed up without a compromise in accuracy.

Keywords: brittle fracture, dynamic phase field model, semi-explicit, parallel computing, domain decomposition, dual partition super-element

1 Introduction

Accurate modelling of fracture processes, especially considering dynamic conditions, is undoubtedly one of most challenging topics in computational solid mechanics. It is also crucial when assessing structures under extreme loading, such as blast and impact. In recent years, phase field modelling has emerged as a popular numerical approach to capture crack initiation and propagation within various materials. The model is rooted in the variational principle for discrete fracture proposed in [1], and its numerical implementation was firstly established in [2] by employing the

Ambrosio-Tortorelli regularisation of sharp discontinuity. This involves an auxiliary field of order parameter that can represent distinct states of material (intact or fractured) with a smooth transition between the two. Notably, the regularised formulation was proved to resemble the gradient damage model [3], and hence the order parameter is also commonly interpreted as damage in literature. The phase field model possesses many computational merits particularly regarding its implementation. This includes exemption of an explicit criterion to track the crack, mesh independency and no introduction of any form of discontinuity. A summary of phase field model and its various extensions can be found in [4].

Despite the aforementioned advantages of the phase field model, its numerical solvability remains a major issue, prompting a significant research focus on this topic in recent years. The reason for this difficulty is two-fold: 1) the non-convexity of the energy functional cannot guarantee convergence to the optimum point by conventional Newton-Raphson search when the system of equations is solved monolithically; and 2) a small element size is typically required to approximate the regularised crack profile, which is governed by a length scale much smaller compared to the size of the domain, leading to a high computational cost.

The former aspect is commonly addressed with a staggered solver [2] but at the cost of excessive iterations. Several nonstandard tracing [5] and optimisation techniques [6] have been adopted to improve the efficiency and robustness of search, mostly tested with quasi-static analysis. Notably, in most quasi-static benchmark numerical examples, the crack is initiated and propagated by prescribing displacement at the loaded end. However, there is a general neglect in the research literature that crack propagation is associated with snap back, which is typically responsible for the lack of convergence rather than the adoption of a monolithic solution procedure. At any rate, under this scenario, dynamic analysis would reflect the real response and perform better numerically with less convergence issues, as also mentioned in [7].

Integration schemes for dynamic phase field modelling can be mainly classified into fully implicit [8], fully explicit [9] and semi-explicit schemes [10,11,12]. For implicit scheme, the equations are temporally integrated without stability limits on the time step size. In a fully explicit scheme, an additional micro-viscous term is necessary to regularise and add time dependency to the damage evolution equation. As no equation solving is involved, its robustness can be guaranteed. However, identifying the micro-viscous parameter and the limit on the time step size would be a main concern. In the semi-explicit scheme, the displacement field is integrated via explicit scheme while the solution for the damage field follows either some external box-constrained optimisation tool [10,11] or a standard Newton-Raphson method [12]. The semi-explicit scheme avoids the ambiguous definition of the micro-viscous parameter and the time step size. In the meantime, the procedure is effectively equivalent to a one-pass staggered scheme.

With regards to the second issue, parallel computation has been explored for enhancing efficiency. In [9], the capability of graphic processing unit (GPU) parallelisation is exploited to accelerate the fully explicit scheme with adaptive time

step control, where quasi-linear scaling is reported in their study. In [13], implicit phase field modelling is tested with a shared memory system in ABAQUS, which reaches optimal efficiency with a relatively limited number of partitions. The staggered and monolithic schemes are compared under a parallel computation framework in [14], where the system is solved with the Krylov-subspace Conjugate Gradient preconditioner as a whole in parallel. Recently, the non-overlapping finite element tearing and interconnecting (FETI) method and its constrained version FETI-DP have been extended to a fully implicit scheme with a staggered solver [7] and a semi-explicit scheme [13] respectively.

This paper extends a previously developed domain decomposition technique based on dual partition super-elements [15] to phase field modelling and compares the performance of the fully implicit and semi-explicit scheme based on the predictor-corrector concept. The introduced domain decomposition framework does not involve any additional dual parameters such as the Lagrangian multiplier used in FETI, and hence it can be readily extended to phase field modelling without modification in the governing equations. In addition, it has the advantage of being hierarchic and hence suitable for hierarchic parallel processing architectures. Furthermore, the approach can be employed in joint with mixed-dimensional coupling and different integration schemes across partitions which could potentially facilitate fracture analysis of large-scale structures using phase field modelling. Following the presentation of the phase field modelling formulation and its incorporation within domain decomposition a numerical example is presented which highlights the relative advantages of the various considered techniques.

2 Mathematical formulations

2.1 Dynamic phase field model formulation

Consider a deformable continuum body in Euclidean space such that it occupies a configuration $\Omega \in \mathbb{R}^{n_{dim}}$, where $n_{dim} = \{1,2,3\}$ at time $t \in \mathcal{T}$, where $\mathcal{T}$ is any time interval of interest $[t_0, t_f]$. According to the least action principle, the actual system configuration must follow the path by minimising the action integral S defined as:

$$S(\mathbf{u}, \phi) = \int_{t_0}^{t_f} \mathcal{L}(\mathbf{u}, \phi)\, dt \tag{1}$$

where $\mathbf{u}(\mathbf{x}, t)$ denotes the displacement field subject to Dirichlet and Neuman boundary conditions such that $\partial\Omega_u \cap \partial\Omega_t = \emptyset$ and $\partial\Omega_u \cup \partial\Omega_t = \partial\Omega$. $\phi(\mathbf{x}, t) \in [0,1]$ denotes an auxiliary scalar damage field which is 0 for intact state and 1 for fully fractured state with irreversibility constraint $\dot{\phi} \geq 0$.

With phase field regularisation, the Lagrangian is defined as:

$$\mathcal{L}(\mathbf{u}, \phi) = \int_\Omega \frac{1}{2} \rho \ddot{\mathbf{u}}.\dot{\mathbf{u}}\, d\Omega - \int_\Omega \psi(\boldsymbol{\varepsilon}(\mathbf{u}), \phi)\, d\Omega + W_{ext} - \int_\Omega G_c \Gamma(\phi, \boldsymbol{\nabla}\boldsymbol{\phi})\, d\Omega \tag{2}$$

where ρ is the material density, $\dot{\mathbf{u}}$ is the velocity field, ψ is the Helmholtz free energy density, $\boldsymbol{\varepsilon} = \mathrm{sym}(\boldsymbol{\nabla}\mathbf{u})$ is the infinitesimal strain tensor, W_{ext} is the external work done by surface tractions $\mathbf{t_n}$ and body force $\mathbf{b}$, G_c is the Griffith fracture energy and γ is the crack density function. To limit the scope of discussion, the standard AT-2 model [2] is adopted within an infinitesimal strain setting and spectral split of the strain energy. The corresponding crack density function and the free energy density expression are given by:

$$\Gamma(\phi, \boldsymbol{\nabla}\boldsymbol{\phi}) = \frac{1}{2}\left[\frac{1}{l_0}\phi^2 + l_0(\boldsymbol{\nabla}\boldsymbol{\phi}.\boldsymbol{\nabla}\boldsymbol{\phi})\right] \tag{3}$$

$$\psi(\boldsymbol{\varepsilon}(\mathbf{u}), \phi) = g(\phi)\mathcal{H}(\boldsymbol{\varepsilon}(\mathbf{u})) + \psi_e^-(\boldsymbol{\varepsilon}(\mathbf{u})) \tag{4}$$

where l_0 is the internal length scale determining the width of the diffusive crack profile, $g(\phi) = (1-\phi)^2$ is the quadratic degradation function [2], $\mathcal{H}(\boldsymbol{\varepsilon}(\mathbf{u}))$ is the maximum history variable used to enforce crack irreversibility, and $\psi_e^-(\boldsymbol{\varepsilon}(\mathbf{u}))$ is the undegraded compressive part of the free energy by spectral split:

$$\mathcal{H}(\boldsymbol{\varepsilon}(\mathbf{u})) = \max_{t_0 \le \tau \le t} \psi^+(\boldsymbol{\varepsilon}(\mathbf{u})) \tag{5}$$

$$\psi^{\pm}(\mathbf{u}) = \frac{1}{2}\lambda_0 \cdot [\langle \mathrm{tr}(\boldsymbol{\varepsilon})\rangle_{\pm}]^2 + \mu\, \langle \varepsilon_i\rangle_{\pm} : \langle \varepsilon_i\rangle_{\pm} \tag{6}$$

in which λ_0 and μ are Lame constants, $\langle \varepsilon_i\rangle_+$ and $\langle \varepsilon_i\rangle_-$ contain the positive and negative principal strains, respectively. By minimising the action integral, the following coupled initial-boundary valued problem (IBVP) is constructed at time t:

$$-\rho\ddot{\mathbf{u}} + \mathrm{div}\,\boldsymbol{\sigma} + \mathbf{b} = 0 \tag{7}$$

$$-g'(\phi)\mathcal{H} - G_c\left[\frac{\phi}{l_0} - l_0\Delta\phi\right] = 0 \tag{8}$$

where $\ddot{\mathbf{u}}$ is the acceleration field, $\boldsymbol{\sigma}$ is the Cauchy stress tensor, Δ is the Laplacian operator. Equations (7) and (8) are accompanied with the following boundary conditions (assuming no Dirichlet boundary conditions imposed on damage field):

$$\boldsymbol{\sigma}\mathbf{n} = \mathbf{t_n} \qquad \text{on } \partial\Omega_t \tag{9}$$

$$\mathbf{u} = \bar{\mathbf{u}} \qquad \text{on } \partial\Omega_u \tag{10}$$

$$\boldsymbol{\nabla}\boldsymbol{\phi}.\mathbf{n} = \mathbf{0} \qquad \text{on } \partial\Omega \tag{11}$$

and initial conditions:

$$\mathbf{u}(\mathbf{x}, 0) = \mathbf{u_0}(\mathbf{x}), \;\; \phi(\mathbf{x}, 0) = \phi_0(\mathbf{x}) \tag{12}$$

2.2 Spatial discretisation

By the standard Galerkin finite element method, the domain is discretised with a mesh Ω^h defined by a finite number n_a of nodes. The solution spaces of two primary fields

$\mathbf{u^h}$ and ϕ^h are then constructed from the continuous piecewise polynomials interpolated at nodal values $\mathbf{u_a}$ and $\boldsymbol{\phi}_\mathbf{a}$:

$$\mathbf{u^h}(x,t) = \sum_{a \in n_a} \mathbf{N_a^u}(x)\mathbf{u_a}(t), \quad \phi^h(x,t) = \sum_{a \in n_a} N_a^{\phi}(x)\phi_a(t) \tag{13}$$

where $\mathbf{N_a^u}(x)$ and $N_a^{\phi}(x)$ are the shape function for displacement and damage fields associated with node a respectively. Conforming to most studies, their expression is assumed to be identical, although employing different shape functions is worth investigation.

Substituting the finite element approximation (13) into the weak form of the initial-boundary valued problem and assembling contributions from all elements through the standard procedure eventually leads to the following semi-discretised nonlinear system of equations:

$$\mathbf{M\ddot{u}} + \mathbf{R_u}(\mathbf{u}, \boldsymbol{\phi}) = \mathbf{P}_u \tag{14}$$

$$\mathbf{R}_{\boldsymbol{\phi}}(\mathbf{u}, \boldsymbol{\phi}) = 0 \tag{15}$$

where $\mathbf{M}$ is the mass matrix, $\mathbf{R_u}$ and $\mathbf{R}_{\boldsymbol{\phi}}$ are internal resistance for displacement and damage fields and $\mathbf{P_u}$ is the external force for displacement. For clear presentation, $\mathbf{u}$ and $\boldsymbol{\phi}$ now denote the vector containing nodal values with the subscript a dropped henceforth, while the viscosity terms can be added easily but ignored here for brevity. Note that the resistance corresponding to the damage field is in unit of energy.

2.3 Temporal discretisation

The time interval $\mathcal{T}$ is discretised into a finite number of time steps $\{t_0, \dots, t_n, t_{n+1}, \dots, t_f\}$. Fields at the n^{th} time step are denoted with subscript n hereafter. Given the states at the previous time step $\{\mathbf{u_n}, \dot{\mathbf{u}}_\mathbf{n}, \ddot{\mathbf{u}}_\mathbf{n}, \phi_n\}$, the goal of integration scheme is to obtain the states at the current step $\{\mathbf{u_{n+1}}, \dot{\mathbf{u}}_\mathbf{n+1}, \ddot{\mathbf{u}}_\mathbf{n+1}, \phi_{n+1}\}$. For a fully implicit scheme, the Hilber-Hughes-Taylor scheme [16] is employed to provide high frequency numerical damping. The system of equations (14) and (15) are now solved at a time within the step controlled by parameter α:

$$\mathbf{M}\ddot{\mathbf{u}}_{n+1} + \mathbf{R_u}(\mathbf{u_{n+1+\alpha}}, \phi_{n+1}) = \mathbf{P}_u(t_{n+1+\alpha}) \tag{16}$$

$$\mathbf{R}_{\boldsymbol{\phi}}(\mathbf{u_{n+1+\alpha}}, \phi_{n+1}) = 0 \tag{17}$$

where the intermediate state at $t_{n+1+\alpha} = t_{n+1} + \alpha\Delta t$ are expressed as

$$\mathbf{u_{n+1+\alpha}} = (1+\alpha)\mathbf{u_{n+1}} - \alpha\mathbf{u_n} \tag{18}$$

The displacement and velocity at current step follow the standard Newmark scheme as:

$$\dot{\mathbf{u}}_{n+1} = \dot{\mathbf{u}}_n + \Delta t[(1-\gamma)\ddot{\mathbf{u}}_n + \gamma\ddot{\mathbf{u}}_{n+1}] \tag{19}$$

$$\mathbf{u}_{n+1} = \mathbf{u}_n + \Delta t\dot{\mathbf{u}}_n + \Delta t^2[(1/2-\beta)\ddot{\mathbf{u}}_n + \beta\ddot{\mathbf{u}}_{n+1}] \tag{20}$$

where the two parameters can be linked to $\alpha \in [-1/3,0]$ as $\gamma = 1/2 - \alpha$ and $\beta = (1-\alpha)^2/4$ [16]. Substituting Equations (18), (19) and (20) into (16) and (17) enables the equations to be expressed in terms of $\ddot{\mathbf{u}}_{n+1}$ and $\boldsymbol{\phi}_{n+1}$, hence solvable either via the monolithic or staggered solver. In this study the monolithic Newton-Raphson procedure is employed. For the benchmark numerical example presented in Section 4, it is observed that under extremely rapid loading, the monolithic solver generally converges well with velocity control. This is because the loading time scale becomes more comparable to the crack propagation speed, thus allowing a larger displacement increment during unstable crack extension.

The proposed semi-explicit scheme resembles the staggered scheme in [6]. Specifically, a prediction of the displacement and velocity field is firstly obtained based on frozen states from the previous step. The damage field is then solved via a Newton-Raphson procedure with driving energy established based on frozen predictors. After convergence is achieved, the corrector is applied with the solved damage field. It is assumed that the step size is sufficiently small such that the correction of displacement has negligible effect on the damage field. The main algorithm is outlined below in Algorithm 1. The limit on the time step size for the mechanical problem can be estimated based on the Rayleigh wave speed as a lower bound since a degraded stiffness reduces the wave speed under most scenarios, though a nonlinear correction factor is still recommended.

Algorithm 1. Semi-explicit phase field model

Input: $\mathbf{u_n}, \dot{\mathbf{u}}_n, \ddot{\mathbf{u}}_n, \boldsymbol{\phi}_n, \Delta t, \gamma, \beta, M$

Output: $\mathbf{u_{n+1}}, \dot{\mathbf{u}}_{n+1}, \ddot{\mathbf{u}}_{n+1}, \boldsymbol{\phi}_{n+1}$

1. Set $t_{n+1} \rightarrow t_n + \Delta t$

2. Estimate predictor displacement $\tilde{\mathbf{u}}_{n+1} = \mathbf{u}_n + \Delta t\dot{\mathbf{u}}_n + \Delta t^2(1/2-\beta)\ddot{\mathbf{u}}_n$

3. Estimate predictor velocity $\tilde{\dot{\mathbf{u}}}_{n+1} = \dot{\mathbf{u}}_n + \Delta t(1-\gamma)\ddot{\mathbf{u}}_n$

4. Set $\boldsymbol{\phi}_{n+1}^{(0)} = \boldsymbol{\phi}_n$ and $j = 0$

5. Solve damage field via Newton-Raphson procedure:

while $\left\|\mathbf{R}_{\boldsymbol{\phi}}\left(\tilde{\mathbf{u}}_{n+1}, \boldsymbol{\phi}_{n+1}^{(j)}\right)\right\| > \mathrm{TOL}$ **do**

Solve $\Delta\boldsymbol{\phi}_{n+1}^{(j)} = \left(\left[\frac{\partial \mathbf{R}_{\boldsymbol{\phi}}}{\partial \boldsymbol{\phi}}\right]^{(j)}\right)^{-1} \mathbf{R}_{\boldsymbol{\phi}}\left(\tilde{\mathbf{u}}_{n+1}, \boldsymbol{\phi}_{n+1}^{(j)}\right)$

Update damage variable $\boldsymbol{\phi}_{n+1}^{(j+1)} = \boldsymbol{\phi}_{n+1}^{(j)} + \Delta\boldsymbol{\phi}_{n+1}^{(j)}$

Set $j \rightarrow j+1$

end while

Set $\phi_{n+1} \rightarrow \phi_{n+1}^{(j)}$

6. Calculate corrector displacement by solving $\frac{1}{\Delta t^2 \beta}\mathbf{M}\Delta\mathbf{u} = -\mathbf{R}_{\mathbf{u}}(\tilde{\mathbf{u}}_{n+1}, \boldsymbol{\phi}_{n+1}) + \mathbf{P}_{\mathbf{u}}$, no equation solving is required if lumped mass matrix is used.

7. Update displacement at current step $\mathbf{u}_{n+1} = \tilde{\mathbf{u}}_{n+1} + \Delta\mathbf{u}$

8. Update acceleration at current step $\ddot{\mathbf{u}}_{\mathbf{n+1}} = \frac{\Delta \mathbf{u}}{\Delta t^2 \beta}$

9. Update velocity at current step $\dot{\mathbf{u}}_{\mathbf{n+1}} = \tilde{\mathbf{u}}_{\mathbf{n+1}} + \Delta t \gamma \ddot{\mathbf{u}}_{\mathbf{n+1}}$

10. Set $t_n \rightarrow t_{n+1}$ and proceed to next step

---

3 Domain decomposition based on dual partition super-elements

The domain decomposition developed in [16] utilises dual super-elements which wrap around the individual partitions referred to as child partitions. The core of the approach is to reduce the size of the global system of equations solved at the higher level via packing and unpacking of the information of child partitions through those super-elements, while utilising parallel processors to solve for the internal degree of freedom (DOF) parameters of the child partitions.

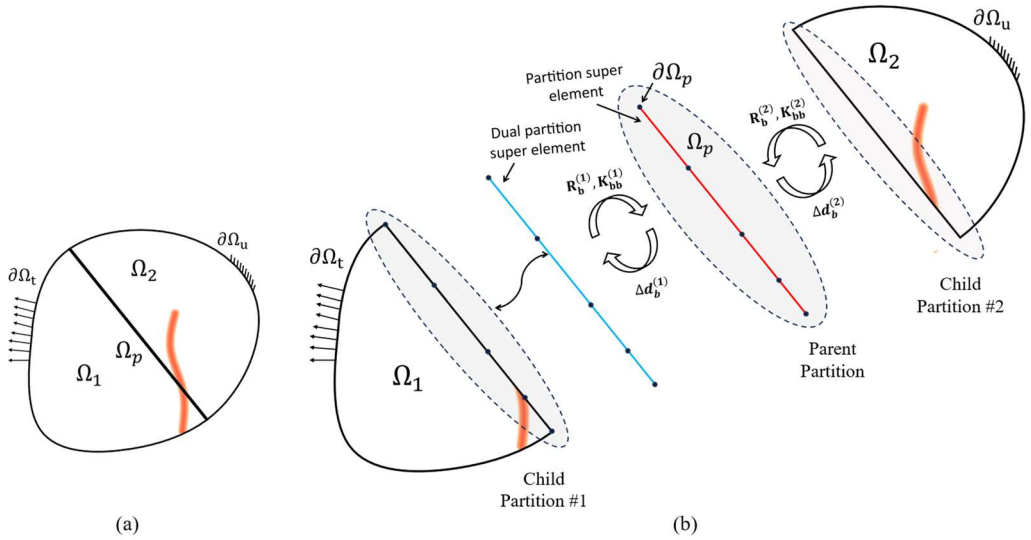

Figure 1: Domain decomposition based on super partition elements: a) original problem; b) partitioning process (dual super elements ignored for partition 2)

Consider the phase field model shown in Figure 1, the overall domain is decomposed into two non-overlapping domains Ω_1 and Ω_2 which are defined as child partitions. For the k^{th} child partition, all nodes are grouped as either inside the partition $N_i^{(k)}$ or on the partition boundary $N_b^{(k)}$. Note the nodes on essential and natural boundaries defined by the IBVP but outside the partition boundary belong to $N_i^{(k)}$. In addition, a parent partition is defined with domain corresponding to the boundary intersected by two child partitions, $\Omega_p = \Omega_1 \cap \Omega_2$. The global governing equations are solved at this level via a Newton-Raphson procedure. For each iteration, the corrections of DOF parameters are calculated as below, where for brevity, an index indicating the current iteration is dropped:

$$\mathbf{K}^{(p)} \Delta \mathbf{d}^{(p)} = -\mathbf{G}^{(p)} \tag{21}$$

where $\mathbf{K}, \mathbf{G}, \mathbf{\Delta d}$ are the general tangent stiffness, out-of-balance force and iterative DOF corrections, and superscript p denotes the parent level. For a fully implicit scheme, $\mathbf{d}$ corresponds to combined displacement and damage freedoms, whereas for a semi-explicit scheme, Equation (21) is solved separately for the iterative corrections of the displacement and damage parameters. Note the stiffness matrix would correspond to lumped mass matrix M for the explicit integration scheme.

To ensure Equation (21) contains information from the overall domain so that it can recover the monolithic analysis with a smaller number of DOFs, the tangent stiffness and resistance forces should be gathered from individual partitions. To achieve this, a super-element (indicated by red line in Figure 1) is defined in the parent partition with its dual part (indicated by the blue line for child partition 1 in Figure 1) also defined for each corresponding child partition to exchange the necessary data. For the scenario considered, the super-element contains nodes on partition boundary.

At assembly stage, the condensed tangent stiffness and resistance forces for each child partition are obtained through forward elimination. The procedure terminates when the local system of equations reaches the following structure:

$$\begin{bmatrix} \mathbf{K}_{\mathbf{ii}}^{(\mathbf{k})} & \mathbf{K}_{\mathbf{ib}}^{(\mathbf{k})} \\ \mathbf{0} & \mathbf{K}_{\mathbf{bb}}^{(\mathbf{k})} \end{bmatrix} \begin{Bmatrix} \mathbf{\Delta d}_{\mathbf{i}}^{(\mathbf{k})} \\ \mathbf{\Delta d}_{\mathbf{b}}^{(\mathbf{k})} \end{Bmatrix} = \begin{Bmatrix} \mathbf{\Delta R}_{\mathbf{i}}^{(\mathbf{k})} \\ \mathbf{\Delta R}_{\mathbf{b}}^{(\mathbf{k})} \end{Bmatrix} \tag{22}$$

This condensation process is performed independently for each child partition, hence taking advantage of parallelisation on multiple processors. The condensed tangent stiffness and resistance forces are then assembled into the system (21) at parent level through communication between child and parent partitions. After the current global iteration is completed, the iterative parameter corrections are then passed back to each partition. The corrections for parameters at the inner nodes are then obtained via back substitution from (22):

$$\mathbf{\Delta d}_{\mathbf{i}}^{(\mathbf{k})} = \left(\mathbf{K}_{\mathbf{ii}}^{(\mathbf{k})}\right)^{-\mathbf{1}} \left(\mathbf{\Delta R}_{\mathbf{i}}^{(\mathbf{k})} - \mathbf{K}_{\mathbf{ib}}^{(\mathbf{k})} \mathbf{\Delta d}_{\mathbf{b}}^{(\mathbf{k})}\right) \tag{23}$$

Again, the procedure is in parallel among all subdomains. Once all freedoms are updated, their resistance and tangent stiffness are re-evaluated and assembled into parent level system according to the procedure described above for next iteration until the global convergence is achieved. Since symmetry of the condensed matrix cannot be ensured, direct solvers such as the Multifrontal solver (MUMPS) [18] are adopted in this study as opposed to iterative solvers with preconditioners. A parallel version of the MUMPs is used for procedures at child level (23) to improve efficiency. For explicit integration scheme, the procedure can be significantly simplified as the displacement DOF parameters are naturally decoupled with a lumped mass matrix.

The approach can be adapted to be hierarchical so that it becomes more compatible with the hierarchical structure of distributed memory HPC systems to reduce the communication cost. More specifically, a nested parent-child structure can be defined across multiple levels. For example, domain 1 in Figure 1 can be further divided into domains 3 and 4 as shown in Figure 2. The structure shown in green acts partially as

local parent partition that gathers information from Ω_3 and Ω_4 while at the same time, it is treated as a child partition that outputs the further condensed stiffness and resistance to the global parent structure indicated in red.

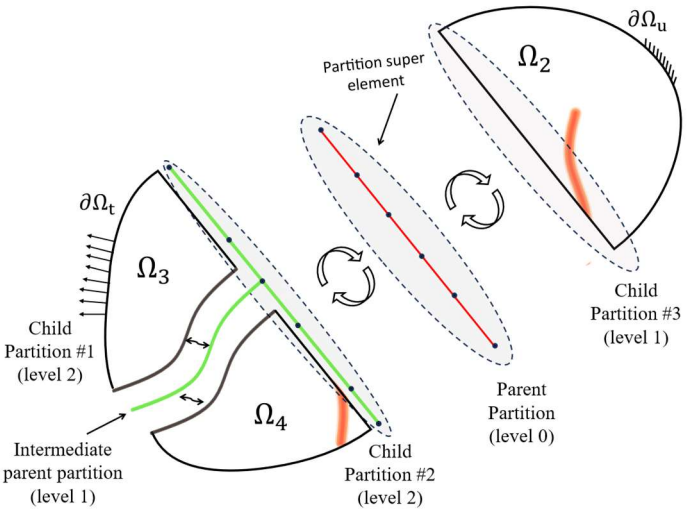

Figure 2: Hierarchical domain decomposition (dual super elements are not shown).

4 Numerical example

The phase field model has been implemented in the nonlinear finite element analysis program ADAPTIC [19]. In this section, a benchmark problem of a single notched plate is examined. The problem configuration is shown in Figure 3, where the plate is fixed at bottom boundary and subjected to constant velocity of 2000 mm/s with lateral restraint at top. The plate thickness is 0.01 mm with out-of-plane movement constrained. A pre-existing crack extended to the middle of the plate is used to initiate the crack. The material and phase field properties are summarised in Table 1, where the values are sourced from references [20] and [11].

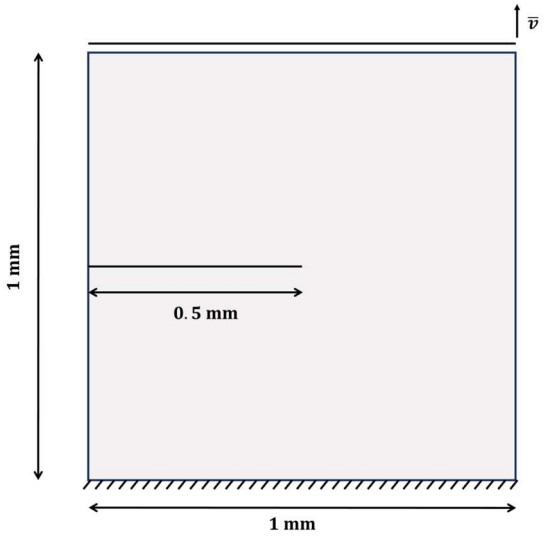

Figure 3: Notched plate problem.

Material Parameters	*Values[Units]*
Young's modulus, E	2.1×10^5 [MPa]
Poisson ratio, ν	0.3 [-]
Material density, ρ	8000 [kg/m^3]
Fracture energy, G_c	2.7 [N/mm]
Length scale, l_0	0.0075 [mm]

Table 1: Material and phase field parameters.

The problem is discretised with 8-noded linear brick elements, and the mesh is refined along the crack path with a minimum element size of 0.002 mm, corresponding to a l_0/h ratio of 3.75. The symmetric monolithic mesh configuration is shown in Figure 4, comprising of 27414 nodes and 13600 elements in total. The partition pattern is generated by the METIS algorithm embedded in the meshing software GMsh [21]. The scenarios under examination are with 4, 8, 16 and 32 partitions, respectively. An additional scenario based on hierarchical partitioning is also considered for the case with 32 subdomains. The four intermediate parent domains contain child partitions indicated by similar colour as shown in Figure 4(f).

The considered total time span is 3.5 μs. For fully implicit analysis, 1000 steps are considered with adaptive step control, where the step size is automatically reduced by factor of 10 when convergence issues are encountered. For semi-explicit analysis, a total of 17500 steps with a step size with 2×10^{-1} s are used. Figure 5 shows crack propagation at different time steps obtained from fully implicit analysis.

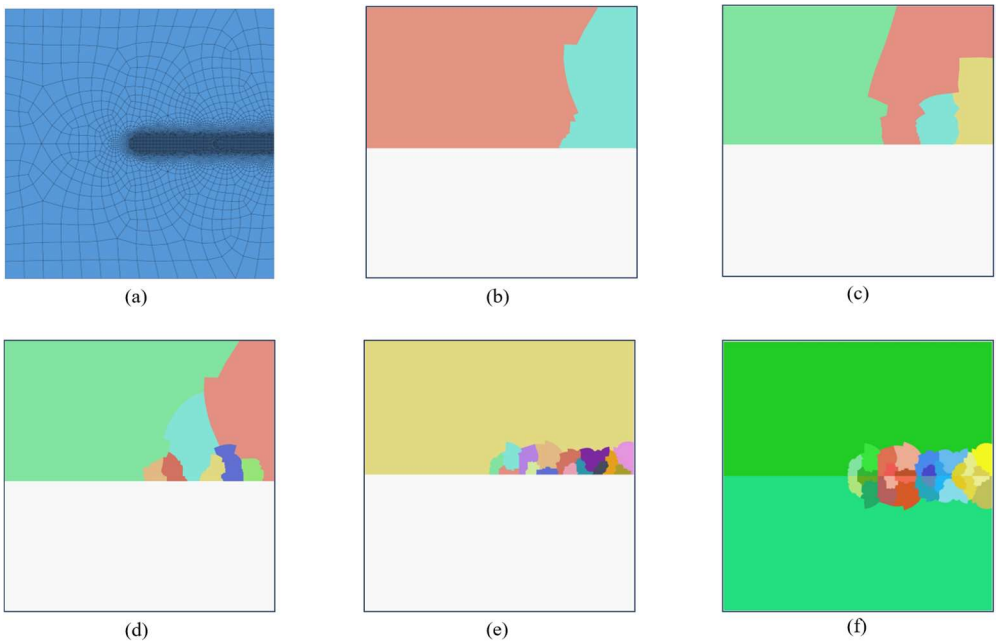

Figure 4: Mesh configuration and partition pattern: a) Monolithic mesh; b) 4 partitions; c) 8 partitions; d) 16 partitions; e) 32 partitions; f) 32 partitions with hierarchical partitioning

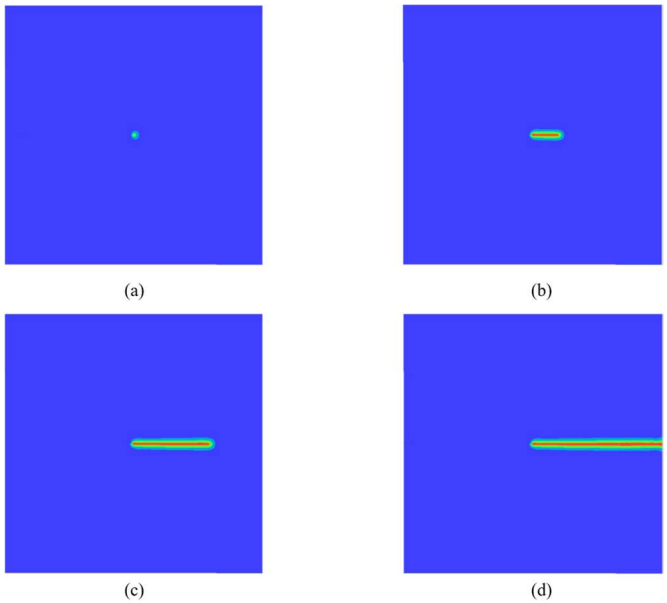

Figure 5: Crack propagation at time a) 2.765µs; b) 2.905µs; c) 3.045µs; d) 3.185µs.

Figure 6 illustrates the variation of the total force applied with the displacement at the top for various scenarios. Initially, the results obtained using a semi-explicit scheme are compared with those from a fully implicit scheme, both conducted with a monolithic mesh. The descending branch of the response exhibits a more gradual slope, attributed to the rapid loading rate. The semi-explicit scheme aligns closely with the fully implicit results, albeit with slight discrepancies on the ascending branch. These deviations become marginally more pronounced in the post-fracture phase, where the two components are completely separated after reaching a displacement of 0.00637 mm. Subsequently, the monolithic analysis results are compared with those derived using domain decomposition. It is observed that the latter approach achieves identical accuracy. This maintained level of accuracy is due to the ability of the partitioned model to fully replicate the original monolithic model without any loss of information via condensation and back substitution.

Figure 7 shows the wall clock time for different scenarios. For fully implicit analysis, the partitioning scheme reaches optimal efficiency with 8 subdomains, at which a speedup of approximately 2 is achieved. It should be noted that apart from the communication overhead, the efficiency of the method also depends on size of problem solved at child and parent level. More partitions lead to a reduction in the DOFs inside each subdomain but increase the size of the system of equations solved at the parent level, and vice versa. The hierarchical partitioning strategy is shown to help with improving efficiency with a larger number of partitions. In this case, a 30% reduction in computational time is recorded for the case of 32 partitions. For the semi-explicit scheme, the results demonstrate a greater speedup. The maximum reduction in wall clock time reaches 89% for the case of 32 partitions. With this scenario, there is a significant reduction in the computing effort at the parent level relative to the child partitions, since only the damage DOFs require the solution of simultaneous equations.

This means that the procedure can benefit more from increasing partitions compared to the fully implicit scheme. Notably, hierarchical partitioning shows a slightly deteriorated performance in this case as an additional intermediate layer is defined.

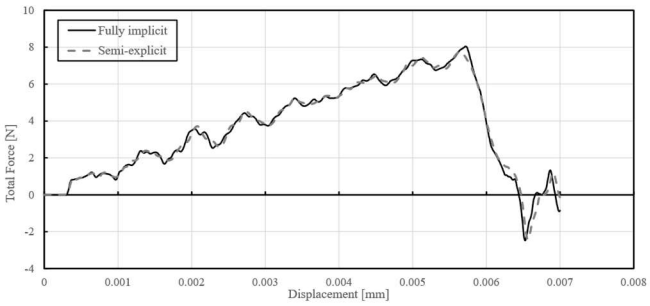

(a)

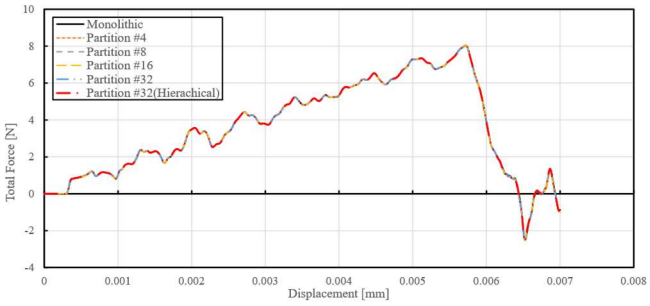

(b)

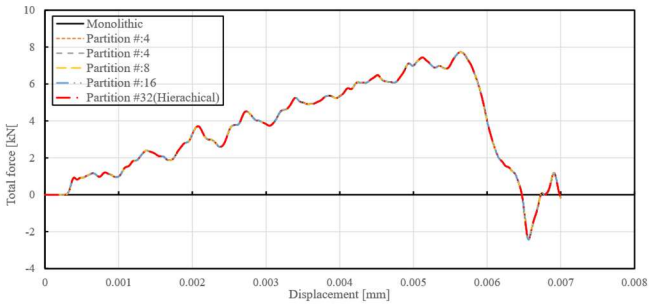

(c)

Figure 6: Plot of total force versus displacement for comparison between a) fully implicit and semi-explicit scheme; b) fully implicit scheme with different number of partitions; c) semi-explicit scheme with different number of partitions

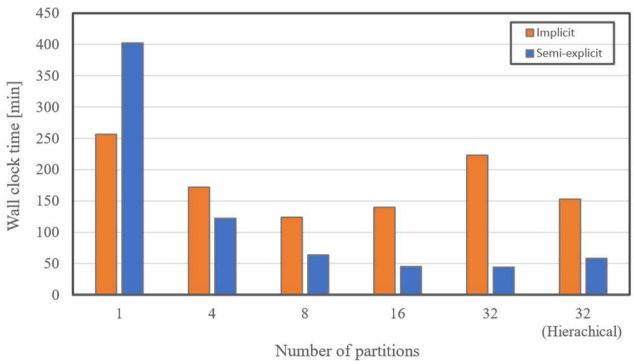

Figure 7: Computational time for different number of partitions

5 Conclusions and Contributions

In this paper, a domain decomposition method is presented to speed up phase field model computations. Together with a semi-explicit scheme, the method can achieve significant speedup with good speedup and accuracy. Several potential extensions are possible, particularly concerning different element dimensions or integration schemes across partitions to further reduce computational cost.

Acknowledgements

The authors would like to acknowledge the funding provided by the Chinese Scholarship Council under grant 202008060195 for supporting doctoral study of the first author.

References

[1] G.A. Francfort, J.-J. Marigo, "Revisiting brittle fracture as an energy minimization problem", Journal of the Mechanics and Physics of Solids, 46, 1319-1342, 1998. DOI: 10.1016/S0022-5096(98)00034-9

[2] B. Bourdin, G.A. "The variational approach to fracture", Journal of Elasticity, 91, 5-148, 2008. DOI: 10.1007/s10659-007-9107-3

[3] R. de Borst, C.V. Verhoosel, "Gradient damage vs phase-field approaches for fracture: Similarities and differences.", Computer Methods in Applied Mechanics and Engineering, 312, 78-94, 2016. DOI: 10.1016/j.cma.2016.05.015

[4] J. Wu, V.P. Nguyen, C.T. Nguyen, D. Sutula, S. Sinaie, S.P.A. Bordas, "Chapter One – Phase-field modelling of fracture.", Advances in Applied Mechanics, 53, 1-183, 2020. DOI: 10.1016/bs.aams.2019.08.001

[5] T. Gerasimov, L. De Lorenzis, "A line search assisted monolithic approach for phase-field computing of brittle fracture.", Computer Methods in Applied Mechanics and Engineering, 312, 276-303, 2016. DOI: 10.1016/j.cma.2015.12.017

[6] P.K. Kristensen, E. Martínez-Pañeda, "Phase field fracture modelling using quasi-Newton methods and a new adaptive step scheme.", Theoretical and Applied Fracture Mechanics, 107, 102446, 2020. DOI: 10.1016/j.tafmec.2019.102446

[7] J. Rannou, C. Bovet, "Domain decomposition methods and acceleration techniques for the phase field fracture staggered solver", HAL Open Science, 2023. Available at: https://hal.science/hal-03938084/

[8] M.J. Borden, C.V. Verhoosel, M.A. Scott, T.J.R. Hughes, C.M. Landis, "A phase-field description of dynamic brittle fracture.", Computer Methods in Applied Mechanics and Engineering, 217-220, 77-95, 2012. DOI: 10.1016/j.cma.2012.01.008

[9] V. Ziaei-Rad. Y. Shen, "Massive parallelisation of the phase field formulation for crack propagation with time adaptivity", Computer Methods in Applied

Mechanics and Engineering, 312, 224-253, 2016. DOI: 10.1016/j.cma.2016.04.013
[10] T.Y. Li, J. -J. Marigo, D. Guilbaud, S. Potapov, "Gradient damage modelling of brittle fracture in an explicit dynamics context", International Journal for Numerical Methods in Engineering, 108, 1381-1405, 2016. DOI: 10.1002/nme.5262
[11] V.P. Nguyen, J. Wu, "Modelling dynamic fracture of solids with a phase-field regularised cohesive zone model", Computer Methods in Applied Mechanics and Engineering, 340, 1000-1022, 2018. DOI: 10.1016/j.cma.2018.06.015
[12] S. Hao, Y. Shen, "An efficient parallel solution scheme for the phase field approach to dynamic fracture based on a domain decomposition method", International Journal for Numerical Methods in Engineering, 125, e7405, 2024. DOI: 10.1002/nme.7405
[13] G. Liu, Q. Li, M.A. Msekh, Z. Zuo, "Abaqus implementation of monolithic and staggered schemes for quasi-static and dynamic fracture phase-field model", Computational Materials Science, 121, 35-47, 2016. DOI: 10.1016/j.commatsci.2016.04.009
[14] M.A. Badri, G. Rastiello, " HPC Finite Element Solvers for Phase-Field Models for Fracture in Solids", in "Numerical Modeling Strategies for Sustainable Concrete Structures. SSCS 2022.", P. Rossi, JL. Tailhan, (Editor), Springer, Cham., 22-32, 2022, DOI: 10.1007/978-3-031-07746-3_3
[15] G.A. Jokhio, B.A. Izzuddin, "A dual super-element domain decomposition approach for parallel nonlinear Finite Element analysis", International Journal for Computational Methods in Engineering Science and Mechanics, 16, 188-212, 2015. DOI: 10.1080/15502287.2015.1043163
[16] H. Hilber, T.J.R. Hughes, R.L. Taylor, "Improved numerical dissipation for time integration algorithms in structural dynamics", Earthquake Engineering & Structural Dynamics, 5, 283-292, 1977. DOI: 10.1002/eqe.4290050306
[17] J.-Y. L'Excellent, "Multifrontal methods: parallelism, memory usage and numerical aspects", Ph.D. dissertation, Ecole normale supérieure de lyon-ENS LYON, Lyon, France, 2012.
[18] B.A. Izzuddin, "Nonlinear dynamic analysis of framed structures", Ph.D. dissertation, Imperial College London, London, United Kingdom, 1991.
[19] C. Miehe, F. Welschinger, M. Hofacker, "Thermodynamically consistent phase-field models of fracture: Variational principles and multi-field FE implementations", International Journal for Numerical Methods in Engineering, 83, 1273-1311, 2010. DOI: 10.1002/nme.2861
[20] C. Geuzaine, J.-F. Remacle, "Gmsh: A 3-D finite element mesh generator with built-in pre- and post-processing facilities", International Journal for Numerical Methods in Engineering, 79, 1309-1331, 2009. DOI: 10.1002/nme.2579